A Discrete-Jointed Robot Model Based Control Strategy for Spatial Continuum Manipulators

Chengshi Wang
Clemson University
Department of Mechanical Engineering
Clemson, SC, USA, 29634
chengsw@clemson.edu

Chase G. Frazelle
Department of Electrical and Computer Engineering
Clemson University
Clemson, SC, USA, 29634
cfrazel@clemson.edu

John R. Wagner
Clemson University
Department of Mechanical Engineering
Clemson, SC, USA, 29634
jwagner@clemson.edu

Ian D. Walker
Clemson University
Department of Electrical and Computer Engineering
Clemson, SC, USA, 29634
iwalker@clemson.edu

***Abstract*— In this paper, a novel strategy is designed for trajectory control of a multi-section continuum robot in three-dimensional space to achieve accurate orientation, curvature, and section length tracking. The formulation connects the continuum manipulator dynamic behavior to a virtual discrete-jointed robot whose degrees of freedom are directly mapped to those of a continuum robot section. Based on this connection, a computed torque control architecture is developed for the virtual robot, for which inverse kinematics and dynamic equations are constructed and exploited, with appropriate transformations developed for implementation on the continuum robot. The control algorithm is implemented on a six degree-of-freedom two-section OctArm continuum manipulator. Experimental results show that the proposed method managed simultaneous extension/contraction, bending, and torsion actions on multi-section continuum robots with decent tracking performance (steady state arc length and curvature tracking error of merely 3.3mm and 0.13m^{-1}, respectively). These results demonstrate that the proposed method can be applied to multi-section continuum manipulators and perform complex maneuvers within a nonlinear setting.**

Keywords*— *Continuum Robot, Forward Kinematics, Inverse Kinematics, Manipulator Dynamics, Motion Control

I. Introduction

Continuum robots [1] are bio-inspired slender hyper-redundant manipulators which present a unique control problem with their theoretically infinite degrees-of-freedom (DoF). Unlike rigid-link manipulators that can only rotate or extend at fixed locations, continuum manipulators can bend at any point along their backbone (see Fig. 1). Recent understanding of biological structures (tongues, tentacles, and elephant trunks) foster continuum robotics research, promising to extend the application of continuum robots into many new environments and providing them with capabilities beyond the scope of their rigid-link counterparts [2], [3]. Success for the practical application of continuum robots heavily depends on the development of real-time controllers that deliver accurate and reliable control. However, the design of high-performance model-based control strategies for continuum robots can be challenging, since the continuum manipulator's kinematic and dynamic models are difficult to derive [4].

Fig. 1. Dynamically controlled OctArm, a pneumatically actuated continuum manipulator with three sections, following a desired configuration trajectory.

Model-based kinematic control of continuum robots has been the subject of extensive research, including the development of both configuration [5], [6], [7], [8], [9], and task space [10], [11] control. Configuration space control provides more stable and faster control performance, whereas task space controller offers the best task accuracy [12]. More complex kinematic formulations for continuum robots such as variable constant curvature (VCC) approximation were used by Mahl et al. in [13] and Wang et al. in [14]. However, static control strategies rely on the steady-state assumption, which impedes fast and accurate motion of continuum robots.

Beyond kinematic control, model-based dynamic controllers that consider the complete kinematics and dynamics of the whole manipulator have been explored by previous researchers [15], [16], [17], [18]. The most challenging field in the control of continuum robots is the development of dynamic controllers that consider the complete dynamics of the whole manipulator. Although difficult to design, model-based dynamic controllers offer faster, more dexterous, more efficient motions, and smoother tracking than model-based kinematics controllers.

Prior research has examined the possibility of controlling a continuum structure via exploiting a "virtual" rigid link robot

model [19], [20], [21]. However, the methodologies were either applied only to planar continuum sections, or formulated using an under-parameterized model which only considers one or two of the possible section motions of bending, extension/contraction, and torsion.

The key contribution of this work is the introduction of a model-based dynamic feedback control architecture that has been specifically designed for controlling continuum robots. We extend our previous work [22] not only from two to three dimensions but also from one to two sections. The novel approach to continuum robot control discussed in this paper is motivated by using a virtual, conventional rigid link robot with discrete joints. The control strategy is developed in the virtual robot coordinates, taking advantage of the well-understood nature of conventional robot dynamics. The virtual robot is selected such that its degrees of freedom are directly mapped to those of the real continuum robot for which control is desired. The work in this paper is the first attempt to accomplish three-dimensional control of continuum robots whose configuration space is parameterized by arc length, curvature, and rotational orientation. Such comprehensive parameterization accounts for simultaneous extension/contraction, bending, and torsion actions of continuum robots, therefore fully matching the control capability and motion complexity of continuum robots.

Specifically, the above approach is validated from model development to hardware implementation for control of a multi-section spatial continuum robot. The continuum section is approximated as a serial rigid-link Revolute-Revolute-Prismatic-Revolute (RRPR) joint spatial robot with an out-of-plane rotation, two in-plane rotations, and a translation in the same plane to create a 3D virtual rigid-link robot [4]. A block diagram of the joint space dynamic controller by feedback linearization for closed-loop configuration space control is depicted in Fig. 2. The control attempts to achieve tracking of configuration space variables (arc length s, curvature κ, and rotational orientation ϕ) using a computed-torque controller in the joint space to calculate virtual torques that are translated into pneumatic pressure in the actuator space. The task space to joint space inverse kinematics are obtained via a desired virtual joint vector which forms the error vector with the actual virtual joint space variables derived from the continuum robot configuration space. The approach mentioned above assumes the constant curvature (CC) approximation [23] for the configuration space.

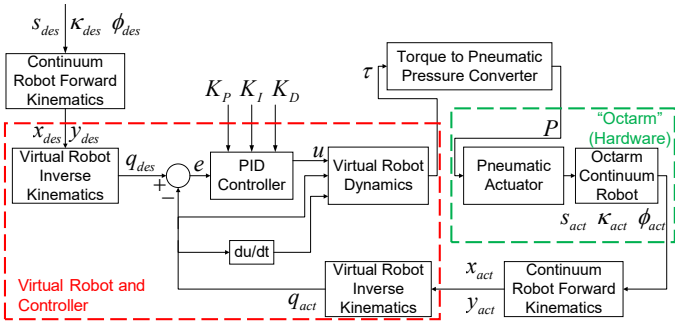

Fig. 2. Block diagram for continuum robot control based on virtual robot models, *des* represents desired trajectories and *act* denotes actual trajectories.

The remainder of the paper is organized as follows. The mathematical forward and inverse kinematics, as well as the dynamics model, are discussed in Section II. The control system design is contained in Section III. The experimental methods, as well as one and two section OctArm experimental results, are discussed in Section IV. Finally, Section V offers conclusions.

II. Mathematical Model

A. Spatial Continuum Robot Forward Kinematics

To quantify the continuum robot movements, a forward kinematic model, which relates the configuration space (backbone shape) variables and task (e.g., tip) space variables, needs to be constructed. Such a model lays the foundation for designing control algorithms and is vital for the practical implementation of continuum robot hardware.

The approach to continuum robot forward kinematics in this article heavily exploits the CC section feature. The CC feature assumes that the configuration space of a three-dimensional (3D) continuum architecture can be parameterized by three variables: arc length s, the curvature $\kappa = 1/r$ as related to the radius r of a curve, and orientation ϕ of the curve plane in space. The CC continuum bending can be decomposed into four discrete motions: (1) a rotation to "point" the tangent at the curve's origin to the curve's end point; (2) a translation from curve origin to end; (3) a second rotation identical with the first to realign with the tangent at the curve's end; and (4) a rotation about the initial tangent; see Fig. 3. Given this observation, a "virtual" 3D four-joint rigid-link RRPR manipulator can be used to model the kinematic transformation along any CC backbone [24]. Consequently, the corresponding continuum robot forward kinematics model can be found using the conventional Denavit-Hartenberg (D-H) [23] convention for the virtual robot; see Table I. The associated homogeneous transformation matrix of the virtual RRPR robot model is given as

$$H_4^0 = \begin{bmatrix} c_1c_2c_4 - c_1s_2s_4 & -s_1 & -c_1c_2s_4 - c_1s_2c_4 & -d_3c_1s_2 \\ s_1c_2c_4 - s_1s_2s_4 & c_1 & -s_1c_2s_4 - s_1s_2c_4 & -d_3s_1s_2 \\ s_2c_4 + c_2s_4 & 0 & -s_2s_4 + c_2c_4 & d_3c_2 \\ 0 & 0 & 0 & 1 \end{bmatrix} \quad (1)$$

where s_l and c_l $(l = 1,2,4)$ denote $\sin(\theta_l)$ and $\cos(\theta_l)$ for the three revolute joints in the RRPR model, respectively and d_3 is the length of the third, prismatic, joint in the RRPR model. The continuum robot kinematics can be readily developed by substituting the joint variables of the virtual robot with the corresponding configuration space variables of a continuous curve. Specifically (see Fig. 3),

$$\theta_1 = \phi, \quad \theta_2 = \theta_4 = \theta, \quad \kappa = \left(\frac{1}{r}\right) \quad (2)$$

We have

$$s = r(2\theta) = \frac{(2\theta)}{\kappa} = \frac{(\theta_2 + \theta_4)}{\kappa} \rightarrow (\theta_2 + \theta_4) = s\kappa \quad (3)$$

$$\frac{d_3}{2} = r\sin\theta = \frac{\sin\theta}{\kappa} \rightarrow d_3 = \frac{2\sin\theta}{\kappa} \quad (4)$$

Substituting (3) and (4) into the model (1) and simplifying gives

$$H_4^0 = \begin{bmatrix} c_\phi c_{s\kappa} & -s_\phi & -c_\phi s_{s\kappa} & \left(c_\phi - c_\phi c_{s\kappa}\right)/\kappa \\ s_\phi c_{s\kappa} & c_\phi & -s_\phi s_{s\kappa} & \left(s_\phi c_{s\kappa} - s_\phi\right)/\kappa \\ s_{s\kappa} & 0 & c_{s\kappa} & s_\kappa/\kappa \\ 0 & 0 & 0 & 1 \end{bmatrix} \quad (5)$$

where c_m and s_m $(m = s, \kappa, \phi, s\kappa)$, denote $\cos(m)$ and $\sin(m)$, respectively. The model (5) describes the forward kinematic relationship (3 by 3 orientation, top left of (5), and 3 by 1 translation, top right) between continuum curve shape (arc length s, curvature κ, and orientation ϕ) and task space (x, y, and z coordinates).

TABLE I
LINK PARAMETERS FOR VIRTUAL RRPR ROBOT MANIPULATOR

LINK	θ	d	a	α
1	θ_1	0	0	90
2	θ_2	0	0	-90
3	0	d_3	0	90
4	θ_4	0	0	-90

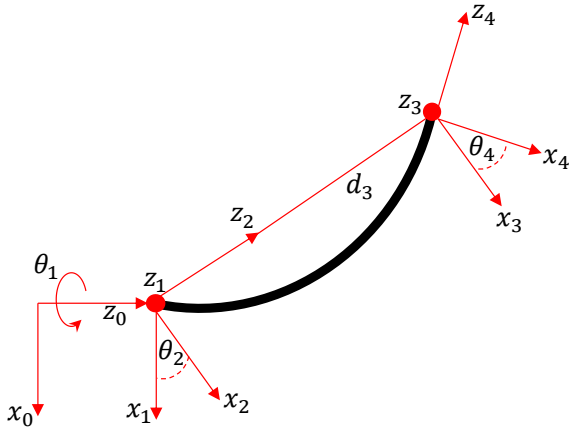

Fig. 3. Three-dimensional constant curvature section geometry obtained via rotation about initial tangent based on virtual RRPR discrete-jointed robot model.

B. Virtual Robot Inverse Kinematics

The inverse kinematics of the continuum robot can be approximated by that of the spatial RRPR virtual robot. After the task space coordinates of the continuum robot are derived from the continuum robot forward kinematics in (5), the x, y, and z coordinates can then be substituted into the inverse kinematics of the RRPR robot model to obtain the desired joint space vector $q_d = [\theta_1 \quad \theta_2 \quad d_3 \quad \theta_4]^T$. From (1) we obtain

$$x = -d_3 c_1 s_2, \quad y = -d_3 s_1 s_2, \quad z = d_3 c_2 \quad (6)$$

Since

$$x^2 + y^2 + z^2 = {d_3}^2 \left[\left(c_1 s_2\right)^2 + \left(s_1 s_2\right)^2 + \left(c_2\right)^2 \right] = {d_3}^2 \quad (7)$$

Thus

$$d_3 = +\sqrt{x^2 + y^2 + z^2} \quad (8)$$

The rotation θ_2 and θ_4 can be obtained from

$$\theta_2 = \tan^{-1}\left(\frac{\mathrm{s}_2}{\mathrm{c}_2}\right) = \tan^{-1}\left(\frac{\sqrt{x^2+y^2}}{d_3} \Big/ \frac{z}{d_3}\right) = \tan^{-1}\left(\frac{\sqrt{x^2+y^2}}{z}\right) = \theta_4 \quad (9)$$

The rotation θ_1 can also be derived as

$$\theta_1 = \tan^{-1}\left(\frac{\mathrm{s}_1}{\mathrm{c}_1}\right) = \tan^{-1}\left(\frac{y}{-d_3 s_2} \Big/ \frac{x}{-d_3 s_2}\right) = \tan^{-1}\left(\frac{y}{x}\right) \quad (10)$$

C. Virutal Robot Dynamics

Incorporating the dynamics of the continuum robot is vital for model-based dynamic control of continuum structures. The dynamic equations of motion, which provide the relationships between actuation and the acceleration, velocity, etc., form the basis for several computational algorithms that are fundamental in control and simulation. In this article, the virtual RRPR rigid-link robot dynamics is derived and exploited to approximate the dynamics of a 3D continuum architecture. For motion control, the dynamic model of a virtual RRPR mechanism is conveniently described by Lagrange dynamics represented in the joint-space formulation.

The Euler-Lagrange dynamics equations of the virtual RRPR manipulator can be written in a matrix form as

$$D(q)\ddot{q} + C(q,\dot{q})\dot{q} + g(q) = \tau \quad (11)$$

where $q \in \mathbb{R}^{4x1}$ is the joint variable vector for the virtual RRPR robot, the joint variables are $q_1 = \theta_1$, $q_2 = \theta_2$, $q_3 = d_3$, and $q_4 = \theta_4$. The vector $\tau \in \mathbb{R}^{4x1}$ is the torque applied to each joint variable. Specifically, the term τ_1 is the applied torque at the first (virtual) revolute joint which drives the orientation of the continuum robot, τ_2 and τ_4 are the applied torques at the (virtual) second and fourth revolute joints which form the shape (curvature) of the continuum robot, and f_3 is the applied force at the third (again, virtual) prismatic joint which elongates/shrinks the continuum robot. The design method of parameters used for virtual rigid-link dynamics modeling is detailed in [25]. The detailed derivation process and derived terms of the inertia matrix $D(q)$, centrifugal and Coriolis matrix $C(q,\dot{q})$ and gravity matrix $g(q)$ in (11) can be found via the link https://urlzs.com/wuEWb for reference.

III. CONTROL SYSTEMS DESIGN

The modeling strategies of the previous section form the basis for control approaches suitable for continuum robots. We seek and exploit simple, relatively computationally inexpensive control methods used in (rigid-link) robot control systems [2] to design the controller in the virtual RRPR robot coordinates. Multiple control methods, such as adaptive control [26], optimal and robust control [27], and learning control [28], are widely used in robotics. Each control method has advantages and disadvantages. However, the main aim of the system is to provide stability and high-frequency updates. In this work, we adopt the computed-torque [29] (feedback linearization plus PID control) approach for the virtual robot, with the sensing and actuation transformed from and to the continuum robot, respectively.

The computed-torque control consists of an inner nonlinear compensation loop and an outer linear control loop with an exogenous control signal, u. This control input converts a complicated nonlinear controller design problem into a simple design problem for a linear system consisting of several decoupled subsystems. One approach to the outer-loop control u is proportional–integral–derivative (PID) feedback. The reason why the PID controller is preferred in this article over the proportional-derivative (PD) controller is that the PID controller eliminates the steady-state error caused by environmental disturbances.

The dynamic model of the virtual robot arm is given in (11). The errors of the robot variables are

$$e = q_d - q,\ \dot{e} = \dot{q}_d - \dot{q},\ \ddot{e} = \ddot{q}_d - \ddot{q} \tag{12}$$

where $e, \dot{e}, \ddot{e}$ express the position, velocity, and acceleration error vectors. The variables $q_d, \dot{q}_d, \ddot{q}_d$ express the desired position, velocity, and acceleration. The torques required for each joint of the virtual robot arm are calculated from (11) and the errors from (12). The linearization is achieved as follows

$$\tau = D(q)\left(\ddot{q}_d - u\right) + C(q,\dot{q})\dot{q} + g(q) \tag{13}$$

The control signal that is obtained from (13) is expressed as follows

$$u = \ddot{q}_d + D^{-1}(q)\left[C(q,\dot{q})\dot{q} + g(q) - \tau\right] \tag{14}$$

If the signal u is selected as the PID feedback controller, then the torque value of each joint will be obtained from (15) and (16).

$$u = -K_d\dot{e} - K_p e - K_i\int e dt \tag{15}$$

$$\tau = D(q)\left(\ddot{q}_d + K_d\dot{e} + K_p e + K_i\int e dt\right) + C(q,\dot{q})\dot{q} + g(q) \tag{16}$$

where K_d is the derivative gain, K_i is the integral gain, and K_p is the proportional gain.

The overall controller of the virtual robot is shown in Fig. 4. The values of the controller gains, i.e., K_d, K_i, and K_p, were determined according to an iterative experimental process to maximize controller performance. The input desired trajectory was represented in terms of Cartesian coordinates x, y, and z, and was calculated from the continuum robot arc length s, curvature κ, and orientation ϕ using the forward kinematics discussed in Section II. Subsequently the virtual robot variables: rotation θ_1, θ_2, d_3, and θ_4 were derived from the inverse kinematics in section II and fed into the control system as a desired reference input signal. Their derivatives and double derivatives were calculated and served as the inputs to the controller through $\mathbb{R}^{4\times1}$ vectors q_d, $\dot{q}_d$, and $\ddot{q}_d$. The output of the controller, u, was then used to establish the torque signal τ along with the systems $D(q)$, $C(q,\dot{q})$, and $g(q)$ matrices. The torque τ was then converted to actuation space in the pressure form and applied to the physical continuum robot system which fed back the current continuum robot shape configuration, subsequently converted to virtual robot rotation and translation $\mathbb{R}^{4\times1}$ signal vectors q and $\dot{q}$ which were then input to the PID controller to form the error and drive the control action.

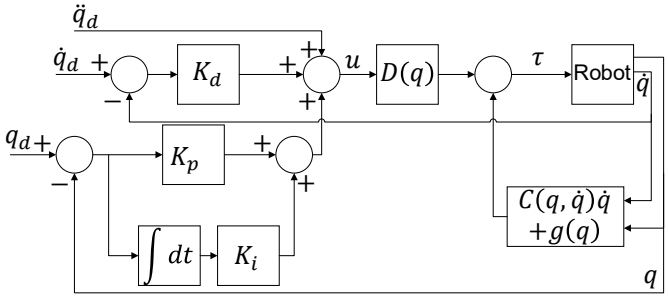

Fig. 4. Block diagram for PID computed-torque controller designed for virtual RRPR robot.

IV. Experimental Implementation

A. Experimental Setup

To demonstrate the validity of the proposed controller based on the virtual rigid-link dynamics model, laboratory experiments were conducted on the tip and mid-sections of the OctArm continuum manipulator [30], [31]. The OctArm, whose physical structure is shown in Fig. 5, is a 9-DoF pneumatically actuated, extensible, continuum robot capable of motion in three dimensions. The kinematically redundant manipulator is comprised of three serially connected sections: base, mid, and tip-section. Each of the three sections can extend (with arc length s) and bend in any direction (with curvature κ and orientation ϕ), providing three DoF for each section. The OctArm is constructed using compressed air-actuated "McKibben" extension artificial muscles with three control channels per section; see Fig. 6 [30]. The OctArm manipulator is equipped with string encoders for length sensing [25].

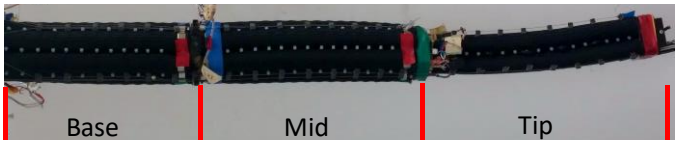

Fig. 5. The OctArm manipulator with base, mid, and tip sections.

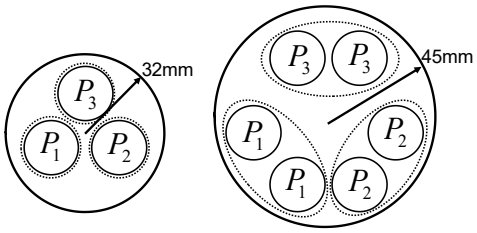

Fig. 6. OctArm actuator cross-section configurations for (a) tip (left), and (b) mid (right) sections (Dotted lines show three control channels)

B. Torque to Pressure Conversion

To facilitate the implementation of the proposed controller into pneumatically actuated continuum architectures like the OctArm, the computed torques $[\tau_1 \quad \tau_2 \quad f_3 \quad \tau_4]^T$ for controlling the virtual rigid-link robot model in (21) must be converted into applied pneumatic pressures onto each of the pneumatic McKibben muscles in the single section. Such a conversion can be inspired by the movements of the OctArm which can be categorized into three distinct motions: (1) extension/contraction which determines the continuum robot arc length s; (2) bending which accounts for the OctArm curvature

κ ; and (3) torsion which translates to continuum robot orientation ϕ.

For pure extension/contraction motion, the calculated extension force f_3 that results from the RRPR model is equally applied to the three muscles to achieve balanced pure extending movement. To generate simultaneous extending, bending, and torsion motions at the single section of the OctArm shown in Fig. 5, the controller generated torques τ_1, τ_2, and τ_4 which are responsible for driving the rotation ϕ and curvature κ. Therefore, the pressure applied to the three McKibben muscle control channels can be represented as

$$\begin{aligned} P_1 &= k_p\left[f_3 + \Delta\tau\cdot\cos\left(\phi + b\cdot\tau_1\right)\right] \\ P_2 &= k_p\left[f_3 + \Delta\tau\cdot\cos\left(\phi + b\cdot\tau_1 + 120^\circ\right)\right] \\ P_3 &= k_p\left[f_3 + \Delta\tau\cdot\cos\left(\phi + b\cdot\tau_1 - 120^\circ\right)\right] \end{aligned} \tag{17}$$

where $\Delta\tau = (\tau_2 + \tau_4)/2$, ϕ denotes the current rotation of the OctArm, k_p is the conversion gain from torque to pressure, and b is a constant. In (17), the terms f_3, $\Delta\tau$, and τ_1 account for extending, bending, and torsion maneuvers, respectively. The difference of pressure given to three distinct sets of control channels will generate a bending effect of constant curvature that matches the continuum robot kinematics model.

C. Two Section OctArm Experiment

The control strategy was implemented on two sections (tip and mid) of the OctArm. Each of these two sections has its own individual 4-DoF virtual RRPR model and each of the two 4-DoF models received control input from separate controllers and generated two unique 4×1 computed torque vectors to actuate each individual section. Two laboratory experiments on the two-sections of the OctArm, each with distinct configuration space settings, are presented here to demonstrate the effectiveness of the new approach in controlling multi-section continuum robots. The model and controller were implemented in the MATLAB/Simulink environment [32]. Interfacing with the OctArm was accomplished using two Quanser Q8-USB data acquisition boards [33]. State estimation of the system was provided through internal measurements of the OctArm via a series of string encoders that run along the length of each section muscle. After output torques and forces were computed from the proposed controller, they were converted to pneumatic pressures via a series of pressure regulators using an output voltage from the Quanser boards. The pressures were then applied onto the corresponding McKibben extension muscles, where one regulator was assigned to one muscle or one muscle pair in the case of the mid-section. A detailed experimental control loop block diagram is illustrated in Fig. 7.

1) Two Section Experiment 1

The desired and configuration space variables for the first experiment, whose video footage link is https://urlzs.com/BLzyj, is shown in Fig. 8. The tip-section arc length, which is desired as a constant 0.38m, demonstrates a 5% overshoot before it reaches steady state with a 3.1 second settling time; the tip-section curvature shows a similar pattern. As for the mid-section, due to the changing center of mass of the tip-section during the experiment, a sawtooth shape of the curvature is observed while the arc length yields a sinusoidal error of $\pm 3.3mm$ with the frequency of orientation ϕ shown in Fig. 9. The full 360° torsional displacement of the mid-section is accomplished smoothly whereas the tip-section orientation shows small sinusoidal fluctuation around the set point due to mid-section rotation. Collectively, the decoupled dynamics model controller demonstrates excellent performance with decent error convergence and fast response in the configuration space. Additional experiments have been conducted in [25], comparing the proposed controller with the conventional static PID controller. The results show that the conventional PID controller has more error and longer rising time, proving the superiority of the proposed controller.

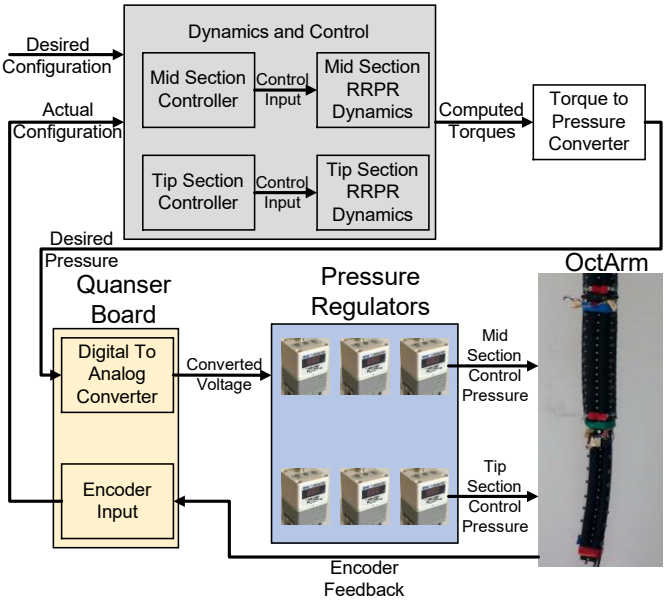

Fig. 7. Experimental control loop block diagram for two section OctArm decoupled virtual discrete-jointed model dynamics control.

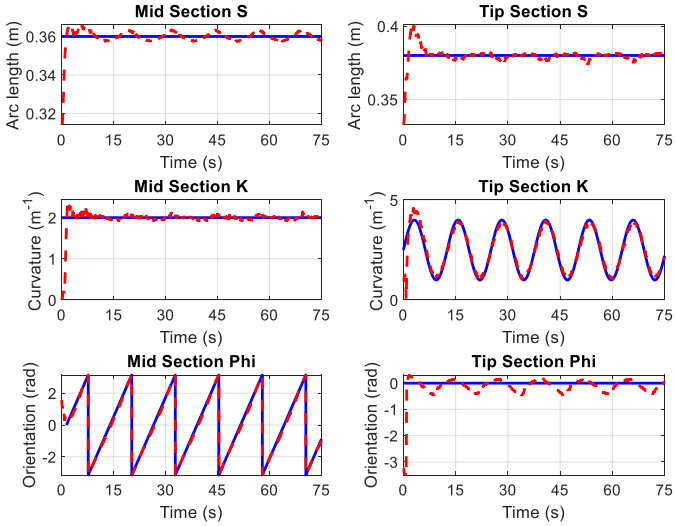

Fig. 8. Two section experiment 1 (OctArm tip and mid sections) — Desired (blue solid line) and actual (red dashed line) arc length s, curvature k, and orientation ϕ in configuration space.

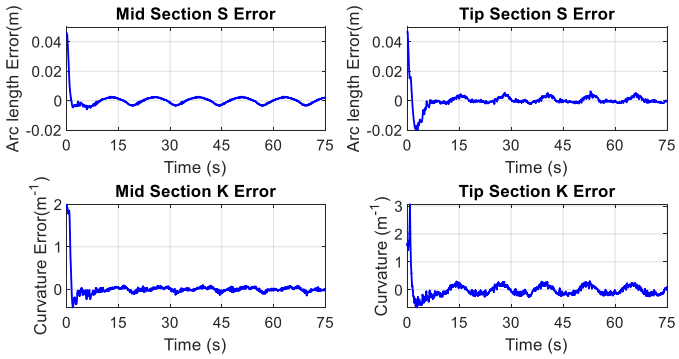

Fig. 9. Two section experiment 1 (OctArm tip and mid sections) — Arc length s, and curvature k error in configuration space.

2) Two Section Experiment 2

After the successful completion of experiment 1, a more complicated two section OctArm maneuver, whose video footage link is https://urlzs.com/k7C98, was tested to examine the control method resilience against demanding robot operations. The desired and actual configuration space variables are exhibited in Fig. 10. The arc length for both tip and mid-section display outstanding performance with minor overshoot on the tip-section. On the other hand, the mid-section curvature exhibits not only oscillatory motion but also high overshoot due to higher stiffness, which leads to mediocre manipulability. The tip-section arc length also experiences intense oscillations at the first sine wave trough and a major overshoot before it reaches a steady state after 22 seconds. Both the tip and mid-section track the desired orientation well. Collectively, the performance of experiment 2 deteriorated compared to that of experiment 1, as shown in Fig. 11, where errors of both section configurations increased by a noticeable amount.

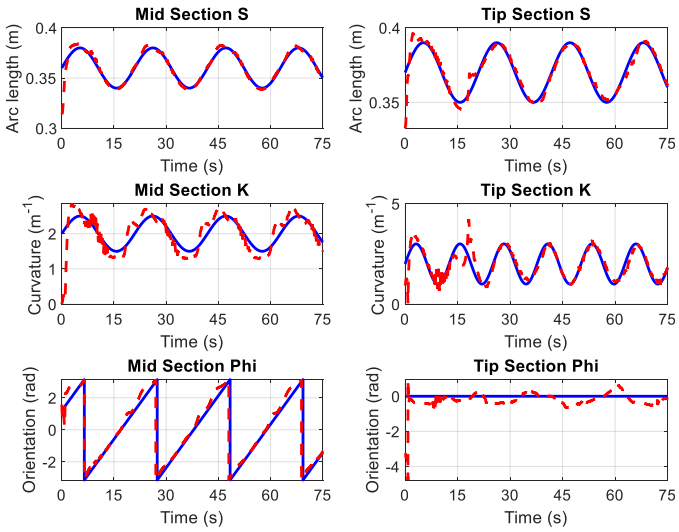

Fig. 10. Two section experiment 2 (OctArm tip and mid sections) — Desired (blue solid line) and actual (red dashed line) arc length s, curvature k, and orientation ϕ in configuration space.

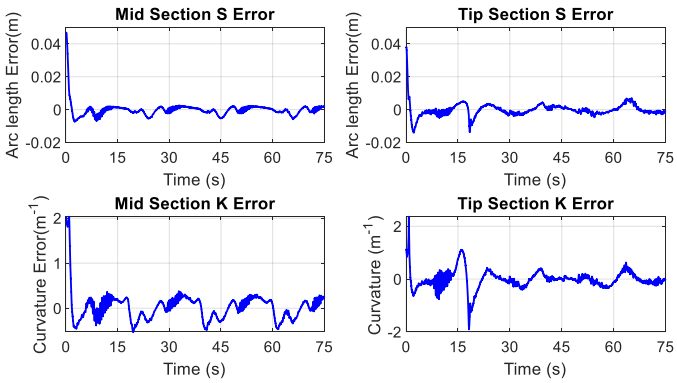

Fig. 11. Two section experiment 2 (OctArm tip and mid sections) — Arc length s, and curvature k error in configuration space.

The joint space variables responses can be found in Fig. 12. The variables θ_{1m}, θ_{2m}, d_{3m}, and θ_{4m} represent the joint space of the mid-section while θ_{1t}, θ_{2t}, d_{3t}, and θ_{4t} denotes that of the tip-section. Due to the high-frequency torques being computed, some oscillatory tracking behavior on the robot curvature related to revolute joints θ_{2m}, θ_{4m}, θ_{2t}, and θ_{4t} is observed before the system reaches steady state at 22 seconds and follows the desired joint space trajectories decently. Like the arc length s behavior, the prismatic joints d_{3m} and d_{3t} demonstrate excellent tracking performance.

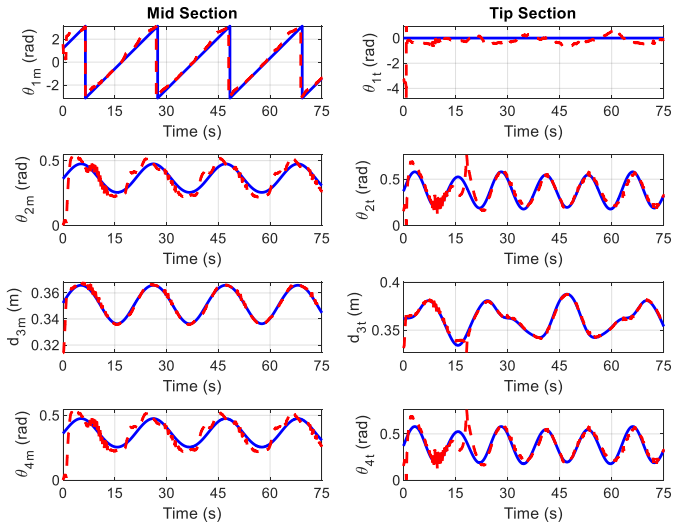

Fig. 12. Two section experiment 2 (OctArm tip and mid sections) — Desired (blue solid line) and actual (red dashed line) θ_{1m}, θ_{2m}, d_{3m}, θ_{4m}, θ_{1t}, θ_{2t}, d_{3t}, and θ_{4t} of the virtual discrete-jointed model in the joint space; the variables θ_{1m}, θ_{2m}, d_{3m}, θ_{4m} represents the mid-section model joint variables and the variables θ_{1t}, θ_{2t}, d_{3t}, θ_{4t} represents the tip-section model joint variables

V. Conclusion

We have introduced a novel model-based dynamic feedback control architecture for extensible multi-section continuum robots. The control law is inspired by conventional rigid link robot computed-torque control techniques. The computed-torque input was translated to pneumatic pressures applied to each pneumatic artificial muscle in the actuator space of the continuum robot through a carefully designed converter. The forward and inverse kinematics, as well as dynamics model approximated by a virtual discrete-jointed robot model, are

derived for both single and two-section continuum robots. The proposed controller was experimentally validated on two sections of the OctArm continuum robot. Accompanying this paper is video footage showing the configuration space tracking motion of the OctArm in 3D space as reported in the experimental results. Future studies should investigate the disturbance rejection capabilities of the proposed control method.

ACKNOWLEDGMENT

This work was supported in part by the U.S. National Science Foundation under grants IIS-1527165 and IIS-1718075, in part by NASA under contract NNX12AM01G, and in part by a NASA Space Technology Research Fellowship, contract 80NSSC17K0173.

REFERENCES

[1] G. Robinson and J. B. C. Davies, "Continuum robots - a state of the art," in *Proceedings 1999 IEEE International Conference on Robotics and Automation (Cat. No.99CH36288C)*, Detroit, MI, USA, 1999, vol. 4, pp. 2849–2854.

[2] R. J. Webster and B. A. Jones, "Design and Kinematic Modeling of Constant Curvature Continuum Robots: A Review," *The International Journal of Robotics Research*, vol. 29, no. 13, pp. 1661–1683, Nov. 2010.

[3] D. Trivedi, C. D. Rahn, W. M. Kier, and I. D. Walker, "Soft robotics: Biological inspiration, state of the art, and future research," *Applied Bionics and Biomechanics*, vol. 5, no. 3, pp. 99–117, Dec. 2008.

[4] I. D. Walker, "Continuous Backbone 'Continuum' Robot Manipulators," *ISRN Robotics*, vol. 2013, pp. 1–19, 2013.

[5] D. B. Camarillo, C. R. Carlson, and J. K. Salisbury, "Configuration Tracking for Continuum Manipulators With Coupled Tendon Drive," *IEEE Trans. Robot.*, vol. 25, no. 4, pp. 798–808, Aug. 2009.

[6] A. Bajo, R. E. Goldman, and N. Simaan, "Configuration and joint feedback for enhanced performance of multi-segment continuum robots," in *2011 IEEE International Conference on Robotics and Automation*, Shanghai, China, May 2011, pp. 2905–2912.

[7] A. Bajo and N. Simaan, "Hybrid motion/force control of multi-backbone continuum robots," *The International Journal of Robotics Research*, vol. 35, no. 4, pp. 422–434, Apr. 2016.

[8] M. Mahvash and P. E. Dupont, "Stiffness Control of Surgical Continuum Manipulators," *IEEE Trans. Robot.*, vol. 27, no. 2, pp. 334–345, Apr. 2011.

[9] A. D. Marchese and D. Rus, "Design, kinematics, and control of a soft spatial fluidic elastomer manipulator," *The International Journal of Robotics Research*, vol. 35, no. 7, pp. 840–869, Jun. 2016.

[10] D. B. Camarillo, C. R. Carlson, and J. K. Salisbury, "Task-Space Control of Continuum Manipulators with Coupled Tendon Drive," in *Experimental Robotics*, vol. 54, O. Khatib, V. Kumar, and G. J. Pappas, Eds. Berlin, Heidelberg: Springer Berlin Heidelberg, 2009, pp. 271–280.

[11] B. Conrad and M. Zinn, "Closed loop task space control of an interleaved continuum-rigid manipulator," in *2015 IEEE International Conference on Robotics and Automation (ICRA)*, Seattle, WA, USA, May 2015, pp. 1743–1750.

[12] T. George Thuruthel, Y. Ansari, E. Falotico, and C. Laschi, "Control Strategies for Soft Robotic Manipulators: A Survey," *Soft Robotics*, vol. 5, no. 2, pp. 149–163, Apr. 2018.

[13] T. Mahl, A. Hildebrandt, and O. Sawodny, "A Variable Curvature Continuum Kinematics for Kinematic Control of the Bionic Handling Assistant," *IEEE Trans. Robot.*, vol. 30, no. 4, pp. 935–949, Aug. 2014.

[14] Hesheng Wang, Weidong Chen, Xiaojin Yu, Tao Deng, Xiaozhou Wang, and R. Pfeifer, "Visual servo control of cable-driven soft robotic manipulator," in *2013 IEEE/RSJ International Conference on Intelligent Robots and Systems*, Tokyo, Nov. 2013, pp. 57–62.

[15] I. A. Gravagne and I. D. Walker, "Uniform regulation of a multi-section continuum manipulator," in *Proceedings 2002 IEEE International Conference on Robotics and Automation (Cat. No.02CH37292)*, Washington, DC, USA, 2002, vol. 2, pp. 1519–1524.

[16] V. Falkenhahn, A. Hildebrandt, and O. Sawodny, "Trajectory optimization of pneumatically actuated, redundant continuum manipulators," in *2014 American Control Conference*, Portland, OR, USA, Jun. 2014, pp. 4008–4013.

[17] A. D. Marchese, R. Tedrake, and D. Rus, "Dynamics and trajectory optimization for a soft spatial fluidic elastomer manipulator," in *2015 IEEE International Conference on Robotics and Automation (ICRA)*, Seattle, WA, USA, May 2015, pp. 2528–2535.

[18] V. Falkenhahn, A. Hildebrandt, R. Neumann, and O. Sawodny, "Dynamic Control of the Bionic Handling Assistant," *IEEE/ASME Trans. Mechatron.*, vol. 22, no. 1, pp. 6–17, Feb. 2017.

[19] Z. Tang, H. L. Heung, K. Y. Tong, and Z. Li, "A Novel Iterative Learning Model Predictive Control Method for Soft Bending Actuators," in *2019 IEEE International Conference on Robotics and Automation (ICRA)*, Montreal, Canada, May 2019, pp. 4004–4010.

[20] R. K. Katzschmann, C. D. Santina, Y. Toshimitsu, A. Bicchi, and D. Rus, "Dynamic Motion Control of Multi-Segment Soft Robots Using Piecewise Constant Curvature Matched with an Augmented Rigid Body Model," in *2019 2nd IEEE International Conference on Soft Robotics (RoboSoft)*, Seoul, Korea (South), Apr. 2019, pp. 454–461.

[21] T. Greigarn, N. L. Poirot, X. Xu, and M. C. Cavusoglu, "Jacobian-Based Task-Space Motion Planning for MRI-Actuated Continuum Robots," *IEEE Robot. Autom. Lett.*, vol. 4, no. 1, pp. 145–152, Jan. 2019.

[22] C. Wang, J. Wagner, C. G. Frazelle, and I. D. Walker, "Continuum Robot Control Based on Virtual Discrete-Jointed Robot Models," in *IECON 2018 - 44th Annual Conference of the IEEE Industrial Electronics Society*, D.C., DC, USA, Oct. 2018, pp. 2508–2515.

[23] M. W. Hannan and I. D. Walker, "Kinematics and the Implementation of an Elephant's Trunk Manipulator and Other Continuum Style Robots," *J. Robotic Syst.*, vol. 20, no. 2, pp. 45–63, Feb. 2003.

[24] M. W. Hannan and I. D. Walker, "Analysis and experiments with an elephant's trunk robot," *Advanced Robotics*, vol. 15, no. 8, pp. 847–858, Jan. 2001.

[25] C. Wang, C. G. Frazelle, J. R. Wagner, and I. Walker, "Dynamic Control of Multi-Section Three-Dimensional Continuum Manipulators Based on Virtual Discrete-Jointed Robot Models," *IEEE/ASME Transactions on Mechatronics*, pp. 1–1, June 2020.

[26] C. G. Frazelle, A. D. Kapadia, and Ian. D. Walker, "A Nonlinear Control Strategy for Extensible Continuum Robots," in *2018 IEEE International Conference on Robotics and Automation (ICRA)*, Brisbane, QLD, May 2018, pp. 7727–7734.

[27] A. D. Kapadia, I. D. Walker, D. M. Dawson, and E. Tatlicioglu, "A Model-based Sliding Mode Controller for Extensible Continuum Robots," in *Proceedings of the 9th WSEAS International Conference on Signal Processing, Robotics and Automation*, Stevens Point, Wisconsin, USA, 2010, pp. 113–120.

[28] D. Braganza, D. M. Dawson, I. D. Walker, and N. Nath, "A Neural Network Controller for Continuum Robots," *IEEE Trans. Robot.*, vol. 23, no. 6, pp. 1270–1277, Dec. 2007.

[29] R. Middletone and G. Goodwin, "Adaptive computed torque control for rigid link manipulators," in *1986 25th IEEE Conference on Decision and Control*, Athens, Greece, Dec. 1986, pp. 68–73.

[30] M. D. Grissom *et al.*, "Design and experimental testing of the OctArm soft robot manipulator," Orlando (Kissimmee), FL, May 2006, p. 62301F.

[31] I. D. Walker *et al.*, "Continuum robot arms inspired by cephalopods," Orlando, Florida, USA, May 2005, p. 303.

[32] "Simulink - Simulation and Model-Based Design." https://www.mathworks.com/products/simulink.html (accessed Jun. 18, 2019).

[33] "Q8-USB Data Acquisition Device - Quanser." https://www.quanser.com/products/q8-usb-data-acquisition-device/ (accessed Jun. 18, 2019).